manuscript No.
(will be inserted by the editor)

Implementation of cellular bulk stresses in vertex models of biological tissues

Shao-Zhen Lin[a,1], **Matthias Merkel**[b,1], **Jean-Francois Rupprecht**[c,1]

[1]Aix Marseille Univ, Université de Toulon, CNRS and Turing Center for Living Systems, Centre de Physique Théorique, Marseille, 13009 (France).

Received: date / Accepted: date

Abstract Vertex models describe biological tissues as tilings of polygons. In standard vertex models, the tissue dynamics results from a balance between isotropic stresses, which are associated with the bulk of the cells, and tensions associated with cell-cell interfaces. However, in this framework it is less obvious how to describe anisotropic stresses arising from the bulk of cells. In epithelia, such bulk anisotropic stresses could arise for instance through medial myosin fluctuations. Two recent publications – Tlili et al., PNAS (2019) and Comelles et al., eLife (2021) – have proposed different schemes to implement bulk anisotropic stresses in vertex models. Here we show that while both schemes transform in the same way under affine deformations, they lead to significantly different tissue dynamics. Our results are consistent with the interpretation that the Tlili et al. scheme describes bulk stresses that are uniform within each cell, while the Comelles et al. scheme corresponds to non-uniform bulk stresses. Finally, we wondered whether a standard vertex model can be fully expressed in terms of bulk cellular stresses alone. We find that, in general, neither scheme can mimic the vertex forces created by cell-cell interface tensions.

Keywords Vertex model · Active stress · Batchelor stress · Multi-scale modeling

1 Introduction

Biological cells convert stored or ambient free energy into mechanical forces that can drive large-scale collective motion such as those observed during developmental processes or wound healing [1]. A central challenge when modeling such processes consists in linking the dynamics across sub-cellular and tissue scales [2]. One set of tools to tackle this challenge are cell-based computational models, including the vertex model. Here, we discuss how sub-cellular mechanical features can be incorporated within the effective vertex model framework, with a focus on isotropic and anisotropic stresses generated by the cytoskeleton within the bulk of the cell.

Vertex models have played a long-standing role in studying the mechanics of living tissues [5,6,7,8,9]. In these models, the dense cellular structure is represented by a tiling of space into polygons. Tissue deformation is described by the motion of polygon corners, called vertices - here labeled by an index i. In common vertex model implementations, the motion of vertex positions $\boldsymbol{r}_i$ is determined by the force balance between pressure (arising from the cell bulk) and tension (arising from the cell-cell interfaces). In practice, this is usually done by expressing both pressure and interface tensions as forces $\boldsymbol{F}_i$ on the vertices.

While several developmental processes have been described in terms of an imbalance of cell pressures and cell-cell interface tensions [10], experimental data also suggest a crucial role for anisotropic stresses arising from within the bulk of the cells. Such bulk anisotropic stresses could be created for instance by polarized medial myosin pulses as they occur during *Drosophila* germ band extension [11] and dorsal closure [12].

While bulk *isotropic* stresses are readily implemented within the vertex model through cell area derivatives [10], implementing bulk *anisotropic* stresses is less straightforward. In this manuscript, we discuss how to map a general symmetric bulk stress tensor $\boldsymbol{\sigma}^{(\mathrm{b})}$ – with both isotropic and anisotropic components – to corresponding vertex forces $\boldsymbol{F}_i^{(\mathrm{b})}$. For a cell with $N \geq 3$

[a]shaozhen.lin@univ-amu.fr
[b]matthias.merkel@univ-amu.fr
[c]*jean-francois.rupprecht@univ-amu.fr

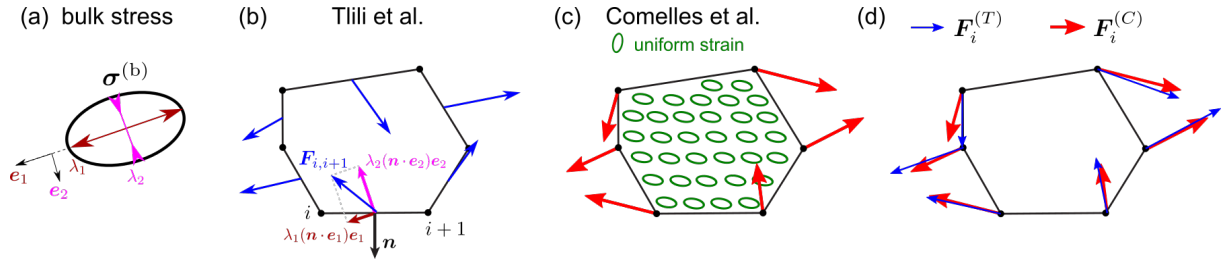

Fig. 1 Sketch of the two schemes considered in this manuscript to define vertex forces based on a bulk cellular stress. (a) Definition of the bulk stress $\boldsymbol{\sigma}^{(\mathrm{b})} = \lambda_1 \mathbf{e}_1 \otimes \mathbf{e}_1 + \lambda_2 \mathbf{e}_2 \otimes \mathbf{e}_2$, outward dark red double arrows indicate an extensile direction (i.e. associated to $\lambda_1 > 0$) and the inward magenta double arrows indicate a contractile direction (i.e. associated to $\lambda_2 < 0$). (b) Tlili et al. scheme [3], with blue arrows indicating the force applied on each interface as defined by Eq. (1). For the junction between the vertices i to $i+1$, we represent the projections of the forces along the extensile (red arrow) and contractile (magenta arrow) directions. (c) Comelles et al. scheme [4], where forces are computed under the assumption of a uniform virtual cellular strain (green ellipses). (d) Comparison of the vertex forces $\boldsymbol{F}^{(T)}$ and $\boldsymbol{F}^{(C)}$, obtained through the Tlili et al. and Comelles et al. schemes, respectively.

vertices, the vertex forces have in total $2 \times N$ components, while the symmetric stress tensor has only 3 independent components. Thus, this problem is generally under-determined, i.e. different sets of forces $\boldsymbol{F}_i^{(\mathrm{b})}$ correspond to the same stress tensor $\boldsymbol{\sigma}^{(\mathrm{b})}$. Hence, what definition for the forces $\boldsymbol{F}_i^{(\mathrm{b})}$ should one choose?

In the recent literature, two different schemes have been proposed to define the forces $\boldsymbol{F}_i^{(\mathrm{b})}$ based on a given bulk stress $\boldsymbol{\sigma}^{(\mathrm{b})}$. Each had its specific motivation: (i) Tlili et al. [3] aimed at understanding the role of patterned cell elongation shaping somites during early zebrafish development, while (ii) Comelles et al. [4] aimed at understanding the experimentally observed anisotropic spreading dynamics of Madin Darby Canine Kidney (MDCK) epithelial monolayers. In this article, we discuss and compare the properties of both schemes.

The article is organized as follows. In Sec. 2, we review the rationales of both schemes. In Sec. 3, we analytically show that both schemes transform in the same way with respect to affine deformations. In Sec. 4, we numerically study how the scheme choice impacts the vertex model dynamics. In Sec. 5, we show that the Tlili et al. scheme can be derived using a similar approach as the Comelles et al. scheme, by just dropping a uniform-strain projection. In our eyes, this means that the Tlili scheme is a more natural choice to describe a bulk stress $\boldsymbol{\sigma}^{(\mathrm{b})}$ that is uniform within each cell (but can differ between cells). We conclude in Sec. 6 by demonstrating that neither scheme is able to express the standard set of vertex model forces of Ref. [6] in terms of isotropic and anisotropic cellular bulk stresses alone.

2 Scheme definitions

2.1 The Tlili et al. (T) scheme

The Tlili et al. scheme relies on Cauchy's stress definition to introduce vertex forces corresponding to a cellular stress $\boldsymbol{\sigma}^{(\mathrm{b})}$ (Fig. 1a). We briefly recall the key ideas of the Tili et al. scheme by considering a single cell with vertices at positions $\boldsymbol{r}_i$, with indices $i = 1, \ldots, N$ ordered in counter-clockwise sense (Fig. 1b).

A homogeneous stress $\boldsymbol{\sigma}^{(\mathrm{b})}$ throughout the cell area corresponds to a force $\boldsymbol{F}_{i,i+1}$ exerted by the cell on the interface $i \to i+1$, which is given by Cauchy's stress theorem as:

$$\boldsymbol{F}_{i,i+1} = -l_{i,i+1} \boldsymbol{n}_{i,i+1} \cdot \boldsymbol{\sigma}^{(\mathrm{b})}, \tag{1}$$

where $l_{i,i+1} = |\boldsymbol{r}_{i+1} - \boldsymbol{r}_i|$ is the length of the interface $i \to i+1$, $\boldsymbol{n}_{i,i+1}$ is the unit vector normal to that interface pointing outside of the cell, and the dot $\cdot$ symbol denotes the inner product. A geometric construction of the force in Eq. 1 is provided in Fig. 1b.

Equation (1) can be transformed into:

$$\boldsymbol{F}_{i,i+1} = -\big[(\boldsymbol{r}_{i+1} - \boldsymbol{r}_i) \times \hat{\boldsymbol{z}} \big] \cdot \boldsymbol{\sigma}^{(\mathrm{b})}, \tag{2}$$

where $\hat{\boldsymbol{z}}$ is the unit vector normal to the cell plane.

Tlili et al. propose to define the resulting force $\boldsymbol{F}_i^{(T)}$ exerted on a given vertex i as the average of the forces exerted on the neighboring interfaces:

$$\boldsymbol{F}_i^{(T)} = \frac{1}{2}(\boldsymbol{F}_{i,i+1} + \boldsymbol{F}_{i-1,i}). \tag{3}$$

We obtain with Eq. (2):

$$\boldsymbol{F}_i^{(T)}(\boldsymbol{\sigma}^{(\mathrm{b})}) = -\boldsymbol{R}_i^{(T)} \cdot \boldsymbol{\sigma}^{(\mathrm{b})}, \tag{4}$$

where we define

$$\boldsymbol{R}_i^{(T)} = \frac{1}{2} (\boldsymbol{r}_{i+1} - \boldsymbol{r}_{i-1}) \times \hat{\boldsymbol{z}}. \tag{5}$$

This is the force definition according to the Tlili et al. scheme.

2.2 The Comelles et al. (C) scheme

The Comelles et al. scheme [4] is based on a virtual work principle. The key idea is that the virtual work δW that the cell exerts via virtual vertex displacements $\delta \boldsymbol{r}_i$ through the cellular bulk stress $\boldsymbol{\sigma}^{(\mathrm{b})}$ can be expressed in two different ways.

The first way is through the vertex displacements:

$$\delta W = \sum_{i \in \mathrm{cell}} \boldsymbol{F}_i^{(C)} \cdot \delta \boldsymbol{r}_i, \tag{6}$$

where $\boldsymbol{F}_i^{(C)}$ are the vertex forces that correspond to the cellular stress $\boldsymbol{\sigma}^{(\mathrm{b})}$.

The second way to express the virtual work δW relies on the effective assumption that the virtual vertex displacements $\delta \boldsymbol{r}_i$ correspond to an affine transformation, i.e. the cell deforms by a uniform virtual strain $\delta \boldsymbol{\varepsilon}$. In this case, the virtual work can also be written as:

$$\delta W = -A \boldsymbol{\sigma}^{(\mathrm{b})} : \delta \boldsymbol{\varepsilon}, \tag{7}$$

where A is the cell area, and the expression $\boldsymbol{\sigma}^{(\mathrm{b})} : \delta \boldsymbol{\varepsilon}$ corresponds to the trace of $\boldsymbol{\sigma}^{(\mathrm{b})} \cdot \delta \boldsymbol{\varepsilon}^{\mathsf{T}}$ with T denoting the transpose operator. Note that here we define the virtual strain tensor $\delta \boldsymbol{\varepsilon}$ as a displacement gradient, which does not need to be symmetric.

The forces $\boldsymbol{F}_i^{(C)}$ can be obtained by equating the virtual work expressions Eqs. (6) and (7). However, the virtual strain $\delta \boldsymbol{\varepsilon}$ first needs to be expressed in terms of $\delta \boldsymbol{r}_i$ before the forces $\boldsymbol{F}_i^{(C)}$ can be deduced by comparison of the coefficients in front of the virtual vertex displacements $\delta \boldsymbol{r}_i$.

To express $\delta \boldsymbol{\varepsilon}$ in terms of $\delta \boldsymbol{r}_i$, Comelles et al. introduce the relative vertex position vectors

$$\boldsymbol{\rho}_i = \boldsymbol{r}_i - \boldsymbol{r}_{\mathrm{C}} \tag{8}$$

with respect to the cell center $\boldsymbol{r}_{\mathrm{C}} = \sum_k \boldsymbol{r}_k / N$.

The Comelles et al. scheme then relies on the assumption of uniform virtual strain $\delta \boldsymbol{\varepsilon}$ (Fig. 1c), which corresponds to

$$\delta \boldsymbol{\rho}_i = \boldsymbol{\rho}_i \cdot \delta \boldsymbol{\varepsilon}. \tag{9}$$

We need to extract $\delta \boldsymbol{\varepsilon}$ with its 4 degrees of freedom from the $2(N-1)$ independent equations in Eq. (9). Whenever the number of vertices N of the cell is strictly larger than 3, this system of equations is over-determined, and thus it has in general no solutions.

Comelles et al. propose to obtain the virtual strain tensor $\delta \boldsymbol{\varepsilon}$ that best matches Eq. (9) through a projection, i.e. a least-squares minimization procedure, which results in:

$$\delta \boldsymbol{\varepsilon} = \boldsymbol{M}^{-1} \cdot \sum_{i \in \mathrm{cell}} \boldsymbol{\rho}_i \otimes \delta \boldsymbol{\rho}_i, \tag{10}$$

with

$$\boldsymbol{M} = \sum_i \boldsymbol{\rho}_i \otimes \boldsymbol{\rho}_i. \tag{11}$$

Here, the symbol $\otimes$ denotes the outer (i.e. dyadic) product. Because $\sum_i \boldsymbol{\rho}_i = 0$, Eq. (10) can be transformed into:

$$\delta \boldsymbol{\varepsilon} = \boldsymbol{M}^{-1} \cdot \sum_{i \in \mathrm{cell}} \boldsymbol{\rho}_i \otimes \delta \boldsymbol{r}_i. \tag{12}$$

Note that the $N \times 2$ elements of $\boldsymbol{M}^{-1} \cdot \boldsymbol{\rho}_i$ correspond to the Moore-Penrose pseudo-inverse of the $2 \times N$ matrix $\boldsymbol{\rho}_i$ [13].

Using Eq. (12) together with the virtual work principle, Eqs. (6) and (7), one obtains

$$\boldsymbol{F}_i^{(C)}(\boldsymbol{\sigma}^{(\mathrm{b})}) = -\boldsymbol{R}_i^{(C)} \cdot \boldsymbol{\sigma}^{(\mathrm{b})} \tag{13}$$

with the definition

$$\boldsymbol{R}_i^{(C)} = A \boldsymbol{\rho}_i \cdot \boldsymbol{M}^{-1}. \tag{14}$$

This corresponds to the expression provided in [4]. Note that in [4], this approach is only discussed for anisotropic (traceless) bulk stress $\boldsymbol{\sigma}^{(\mathrm{b})}$.

2.3 Consistency checks

We first checked that for symmetric bulk stress $\boldsymbol{\sigma}^{(\mathrm{b})}$, both schemes create neither any net force nor any net torque on a cell (Appendix B.1).

Moreover, we checked that for any given (input) bulk stress $\boldsymbol{\sigma}^{(\mathrm{b})}$, both schemes yield identical (output) cell stresses as defined through the Batchelor formula [14,15,16]

$$\boldsymbol{\sigma}_B[\boldsymbol{F}_i] = -\frac{1}{A} \sum_{i \in cell} \boldsymbol{r}_i \otimes \boldsymbol{F}_i. \tag{15}$$

In Appendix B.2, we show that indeed:

$$\boldsymbol{\sigma}_B\left[\boldsymbol{F}_i^{(T)}(\boldsymbol{\sigma}^{(\mathrm{b})})\right] = \boldsymbol{\sigma}_B\left[\boldsymbol{F}_i^{(C)}(\boldsymbol{\sigma}^{(\mathrm{b})})\right] = \boldsymbol{\sigma}^{(\mathrm{b})}. \tag{16}$$

Hence, even though both schemes define different forces, they correspond to the same Batchelor stress.

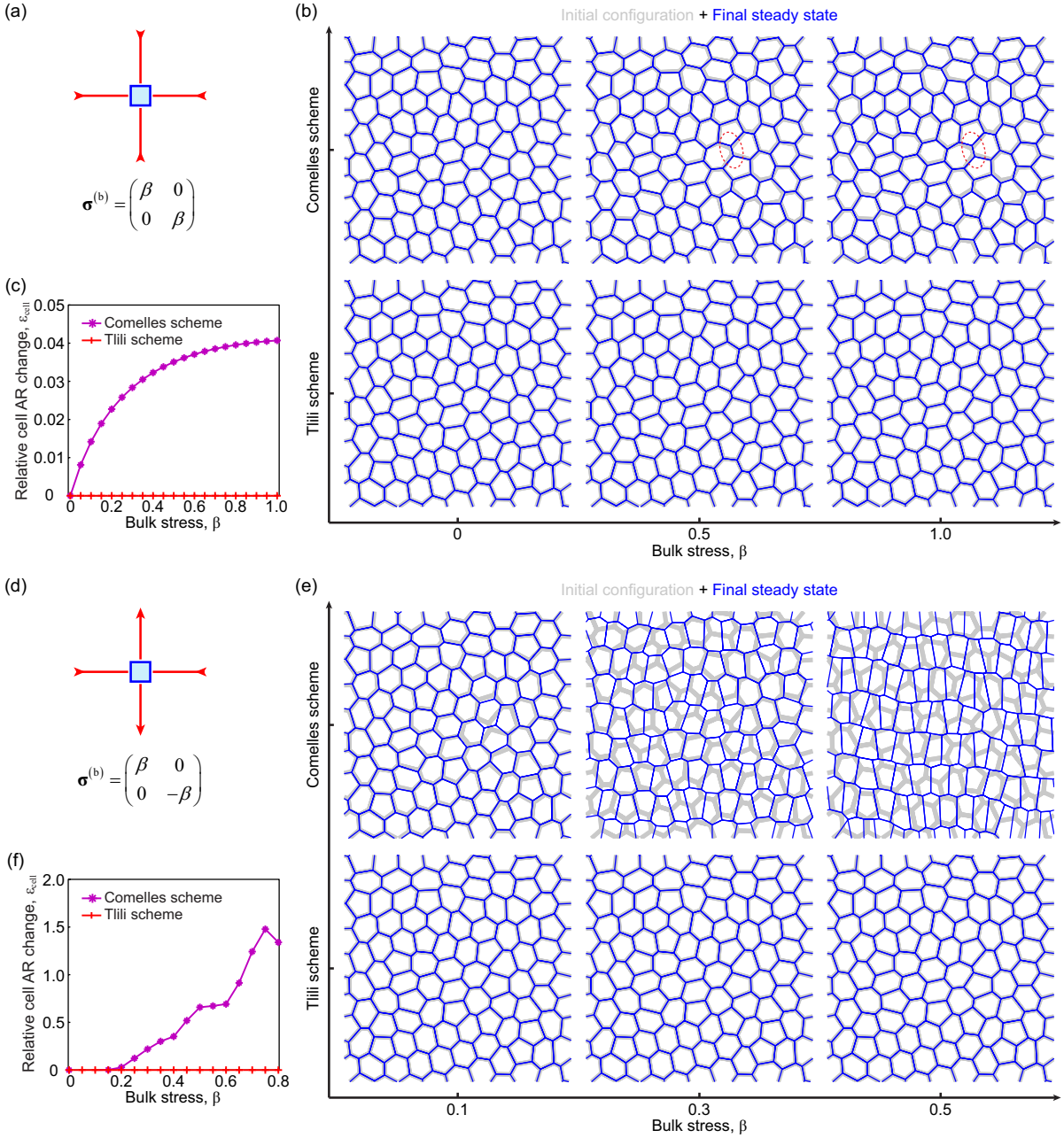

Fig. 2 Behavior of a cell sheet with periodic boundary conditions in the presence of (top row; a-c) uniform isotropic bulk stress $\boldsymbol{\sigma}^{(\mathrm{b})} = \beta \boldsymbol{I}$ (bottom row; d-f) uniform anisotropic bulk stress $\boldsymbol{\sigma}^{(\mathrm{b})} = \beta\,(\boldsymbol{e}_x \otimes \boldsymbol{e}_x - \boldsymbol{e}_y \otimes \boldsymbol{e}_y)$, which is contractile in the x and extensile in the y direction. (a,d) Geometry and bulk stress orientation. (b,e) Snapshots of typical tissue configurations obtained through (top row) the Comelles scheme and (bottom row) the Tlili scheme for increasing values of the imposed bulk stress (b: $\beta = 0, 0.5, 1.0$; e: $\beta = 0.1, 0.3, 0.5$). Shown are initial (gray) and final (blue) stationary states. In panel b, changes in the configuration are highlighted by red ellipses. (c, f) Relative cell aspect ratio (AR) change $\varepsilon_{\mathrm{cell}}$ as a function of the bulk stress β. The aspect ratio change is defined based on the cell shape tensor $\boldsymbol{M}$ defined in Eq. (11) (see Appendix A). Simulation parameters are provided in Table 1.

3 Both schemes transform in the same way under affine cell deformations

Here we show that both schemes transform in the same way under an affine transformation $\boldsymbol{G}$ applied to the cell shape. To this end, we first define the deformed cell shape, where we map each vertex $\boldsymbol{r}_i$ of a cell to $\boldsymbol{r}_i'$ with:

$$\boldsymbol{r}_i' = \boldsymbol{G} \cdot \boldsymbol{r}_i. \tag{17}$$

To study the effect of this transformation, we insert it in the definitions of the vectors $\boldsymbol{R}_i^{(T)}$ and $\boldsymbol{R}_i^{(C)}$ – which define the Tlili and Comelles et al. schemes in

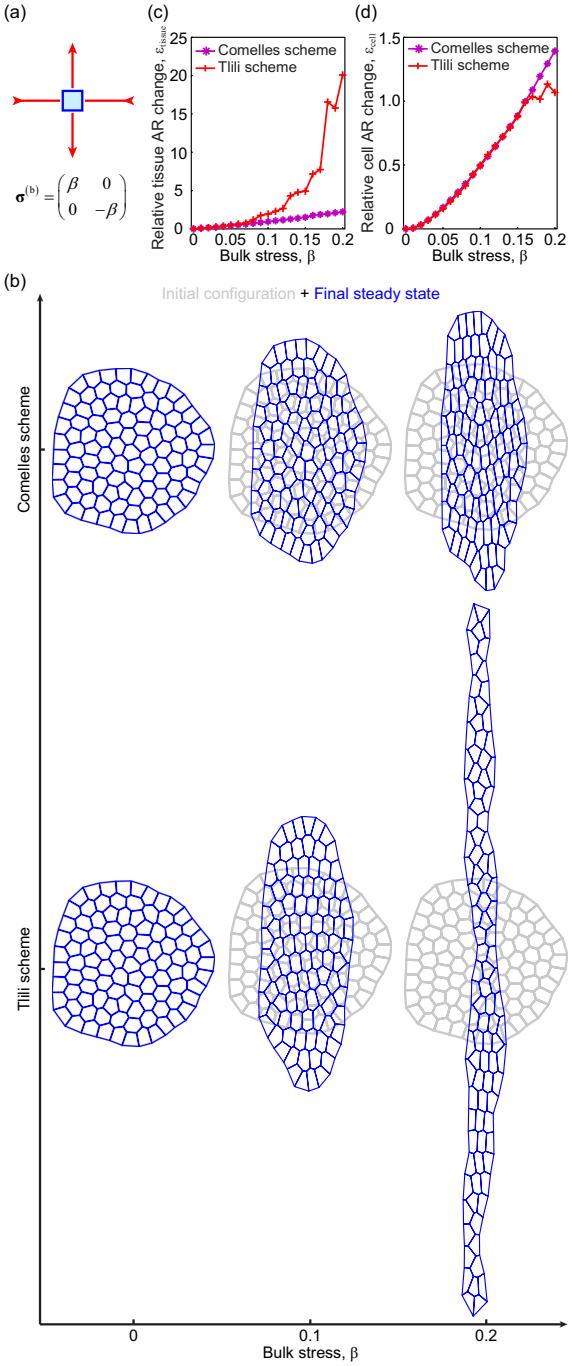

Fig. 3 Vertex model simulations of a cell aggregate with free boundary conditions in the presence of a uniform bulk anisotropic stress $\boldsymbol{\sigma}^{(\mathrm{b})} = \beta\,(\boldsymbol{e}_x \otimes \boldsymbol{e}_x - \boldsymbol{e}_y \otimes \boldsymbol{e}_y)$. (a) Sketch of the anisotropic bulk stress. (b) Comparison of the final tissue morphology using the Comelles et al. (top row) and the Tlili et al. (bottom row) schemes for increasing bulk stresses $\beta = 0, 0.1, 0.2$. (c, d) Relative changes of tissue aspect ratio (AR) $\varepsilon_{\text{tissue}}$ (c) and of cell aspect ratio $\varepsilon_{\text{cell}}$ (d) as a function of the bulk stress β. Both $\varepsilon_{\text{tissue}}$ and $\varepsilon_{\text{cell}}$ are defined based on the cell shape tensor $\boldsymbol{M}$ in Eq. (11) (see Appendix A). Simulation parameters are provided in Table 1.

(5) and (14), respectively – to obtain their transformed versions, $\boldsymbol{R}_i^{(T)\prime}$ and $\boldsymbol{R}_i^{(C)\prime}$.

We obtain the following Tlili et al. vectors for the transformed cell:

$$\begin{aligned} R_{i,\gamma}^{(T)\prime} &= \frac{1}{2} G_{\alpha\beta}\,(r_{i+1,\beta} - r_{i-1,\beta})\,\varepsilon_{\alpha z\gamma}, \\ &= R_{i,\alpha}^{(T)}\,\mathrm{CM}(\boldsymbol{G}^{\mathsf{T}})_{\alpha\gamma}. \end{aligned} \tag{18}$$

Here, ε is the Levi-Civita symbol and $\mathbf{CM}(\boldsymbol{G}^{\mathsf{T}})$, and the cofactor matrix of $\boldsymbol{G}^{\mathsf{T}}$ (transpose of $\boldsymbol{G}$) is defined as

$$\mathbf{CM}(\boldsymbol{G}^{\mathsf{T}}) = \begin{pmatrix} G_{yy} & -G_{xy} \\ -G_{yx} & G_{xx} \end{pmatrix}. \tag{19}$$

In deriving Eq. (18), we used the identity $G_{\alpha\beta}\varepsilon_{\alpha z\gamma} = \varepsilon_{\beta z\alpha}\,\mathrm{CM}(\boldsymbol{G}^{\mathsf{T}})_{\alpha\gamma}$, which can be verified component–wise.

We obtain the following Comelles et al. vectors for the transformed cell:

$$\begin{aligned} \boldsymbol{R}_i^{(C)\prime} &= \det(G)\,A\,\boldsymbol{\rho}_i \cdot \boldsymbol{G}^{\mathsf{T}} \cdot \boldsymbol{G}^{\mathsf{T}\,-1} \cdot \boldsymbol{M}^{-1} \cdot \boldsymbol{G}^{-1}, \\ &= \boldsymbol{R}_i^{(C)} \cdot \mathbf{CM}(\boldsymbol{G}^{\mathsf{T}}). \end{aligned} \tag{20}$$

Here, we used in the first step that the mapped area and relative vertex positions are $A' = \det(G)\,A$ and $\boldsymbol{\rho}_i' = \boldsymbol{G} \cdot \boldsymbol{\rho}_i$, and in the second step we used $\boldsymbol{G}^{-1} = \mathbf{CM}(\boldsymbol{G}^{\mathsf{T}})/\det(G)$.

Eqs. (18) and (20) show that both Tlili et al. and Comelles et al. vectors transform according to the very same rule under any affine transformation applied to a given cell. Moreover, we show in Appendix C.1 that both the Tlili and Comelles et al. schemes coincide for regular polygons. As a consequence, the Tlili et al. and Comelles et al. forces will coincide for any cell shape that results from an affine transformation of a regular polygon – independently of the bulk stress tensor $\boldsymbol{\sigma}^{(\mathrm{b})}$.

Nevertheless, as we will see in the following section, both schemes lead to different vertex model dynamics.

4 Numerical results: both schemes lead to different dynamics

In this section, we study the dynamics of a vertex model where we combine standard vertex model forces [7,17], denoted $\boldsymbol{F}_i^{(\mathrm{svm})}$, with forces induced by a bulk stress $\boldsymbol{\sigma}^{(\mathrm{b})}$, denoted $\boldsymbol{F}_i^{(x)}(\boldsymbol{\sigma}^{(\mathrm{b})})$, into the following expression for the total force exerted on a vertex i:

$$\boldsymbol{F}_i^{(\mathrm{total})} = \boldsymbol{F}_i^{(\mathrm{svm})} + \boldsymbol{F}_i^{(x)}(\boldsymbol{\sigma}^{(\mathrm{b})}). \tag{21}$$

Here, $x \in \{C, T\}$, i.e. $\boldsymbol{F}_i^{(x)}(\boldsymbol{\sigma}^{(\mathrm{b})})$ is defined either according to the Tlili or the Comelles scheme.

The standard vertex model forces $\boldsymbol{F}_i^{(\mathrm{svm})}$ in the first term are defined using the effective work function [7]:

$$U = \frac{1}{2} K_A (A - A_0)^2 + \frac{1}{2} K_P \big(P - P_0\big)^2. \tag{22}$$

Here, A, P are cell area and perimeter, A_0, P_0 are parameters corresponding to preferred cell area and perimeter, and K_A, K_P are the associated moduli. Parameter values used are listed in Table 1. The corresponding standard vertex model force applied on any given vertex i is $\boldsymbol{F}_i^{(\mathrm{svm})} = -\partial U/\partial \boldsymbol{r}_i$.

We use friction-based dynamics [10] with a uniform friction coefficient γ:

$$\gamma \frac{\mathrm{d}\boldsymbol{r}_i}{\mathrm{d}t} = \boldsymbol{F}_i^{(\mathrm{total})}. \tag{23}$$

We initialize our system with a Voronoi tessellation of $N = 100$ cell centroids at random locations either (i) within a square of side length $\sqrt{NA_0}$ with periodic boundary conditions [18], or (ii) within a circle of radius $\sqrt{NA_0}$. For (i) we keep the system size fixed during the simulation, while for (ii) we use free boundary conditions. In both cases, we run the system with $\boldsymbol{\sigma}^{(\mathrm{b})} = \mathbf{0}$ until there is no significant change in the vertex positions (i.e. maximal vertex speed $< 10^{-4}$). Afterwards, we set the same value $\boldsymbol{\sigma}^{(\mathrm{b})} \neq \mathbf{0}$ in all cells and let the system relax again until there is again no significant change in the vertex positions.

Isotropic $\boldsymbol{\sigma}^{(\mathrm{b})}$. We first consider the case where the bulk cellular stress is isotropic (Fig. 2a):

$$\boldsymbol{\sigma}^{(\mathrm{b})} = \beta \boldsymbol{I} = \beta(\boldsymbol{e}_x \otimes \boldsymbol{e}_x + \boldsymbol{e}_y \otimes \boldsymbol{e}_y), \tag{24}$$

where $\boldsymbol{I}$ is the unit tensor in two dimensions.

For periodic boundary conditions, no vertex displacements are observed between initial and final states when using the Tlili et al. scheme. In contrast, using the Comelles et al. scheme results in small changes of the cell aspect ratios, see Fig. 2b-c.

Anisotropic $\boldsymbol{\sigma}^{(\mathrm{b})}$. We now consider an anisotropic bulk cellular stress of the form (Fig. 2d)

$$\boldsymbol{\sigma}^{(\mathrm{b})} = \beta \left(\boldsymbol{e}_x \otimes \boldsymbol{e}_x - \boldsymbol{e}_y \otimes \boldsymbol{e}_y\right). \tag{25}$$

For $\beta > 0$, the latter definition corresponds to a contractile stress in the x direction combined with an extensile stress in the y direction.

For periodic boundary conditions, no vertex displacements are observed when using the Tlili et al. scheme. In contrast, using the Comelles et al. scheme results in a net elongation of cells, see Fig. 2e-f and Movie 1. These results are in line with those obtained for isotropic $\boldsymbol{\sigma}^{(\mathrm{b})}$ (Fig. 2b-c).

These results suggest that only the Tlili et al. scheme is consistent with the expectation that, in a periodic domain, the application of a spatially homogeneous bulk stress $\boldsymbol{\sigma}^{(\mathrm{b})}$ (i.e. same bulk stress in all cells *and* uniform bulk stress within each cell) should not result in any net vertex force. Indeed, if all cells surrounding a given vertex i have equal bulk stress, then the corresponding Tlili forces on the vertex i sum up to zero as a direct consequence of the Tlili force definition Eq. (4). Conversely, the initially force-balanced state changes when turning on the Comelles forces, which indicates that there are additional net forces on individual vertices, even though $\boldsymbol{\sigma}^{(\mathrm{b})}$ is the same for all cells. In this sense, the Comelles scheme can be interpreted as corresponding to a non-uniform intra-cellular bulk stress.

Finally, we also studied a free standing cell aggregate with free boundary conditions under the effect of the same bulk anisotropic stress as before, Eq. (25). We observe an overall tissue elongation along the y axis for both schemes (Fig. 3b,c and Movies 2,3). However, while the average cell aspect ratio is similar for both schemes (Fig. 3d), the overall tissue elongation is significantly larger for the Tlili et al. scheme (Fig. 3c). Indeed, compared to the Comelles scheme, the Tlili et al. scheme favors cell-cell rearrangements through T1 transitions.

Taken together, we find that the choice of the scheme to translate bulk cellular stresses into vertex forces can have a strong impact on the vertex model dynamics. Given that both schemes behave the same for cell shapes that are affinely deformed regular polygons, these differences must arise from non-affinities in the cell shape. This is also exemplified in Appendix C.2.

5 The Tlili scheme can be derived like the Comelles scheme without a uniform-strain projection

Here we use the virtual work principle as in Sec. 2.2 to demonstrate that the Tlili et al. scheme can be derived like the Comelles et al. scheme, but without the uniform-strain projection.

We focus on a single cell with virtual vertex displacements $\delta \boldsymbol{r}_i$. In analogy to Eq. (6), we express the virtual work δW carried out by the cell through the cellular stress $\boldsymbol{\sigma}^{(\mathrm{b})}$ as

$$\delta W = \sum_{i \in \mathrm{cell}} \boldsymbol{F}_i^{(X)} \cdot \delta \boldsymbol{r}_i. \tag{26}$$

The label (X) indicates that $\boldsymbol{F}_i^{(X)}$ can be different from the $\boldsymbol{F}_i^{(C)}$ set of forces, since we will modify the Comelles et al. derivation to avoid the need for the uniform-strain projection.

As in Comelles et al., we equate the virtual work expression Eq. (26) with an expression combining the stress $\boldsymbol{\sigma}^{(\mathrm{b})}$ and the virtual strain $\delta\boldsymbol{\varepsilon}$. However, in contrast to Comelles et al. we allow for a spatially varying

strain field

$$\delta W = -\int_A \boldsymbol{\sigma}^{(\mathrm{b})} : \delta\boldsymbol{\varepsilon}\, \mathrm{d}A = -\boldsymbol{\sigma}^{(\mathrm{b})} : \left(\int_A \delta\boldsymbol{\varepsilon}\, \mathrm{d}A\right), \quad (27)$$

where the integral is over the whole cell area A.

Using a version of Gauss divergence theorem discussed e.g. in Ref [19], the area integral of the virtual strain in Eq. (27) can be expressed as a contour integral around the cell outline

$$\begin{aligned}\int_A \delta\boldsymbol{\varepsilon}\, \mathrm{d}A &= \oint_{\partial A} \boldsymbol{n} \otimes \delta\boldsymbol{r}\, \mathrm{d}\ell \\ &= \sum_{i\in\mathrm{cell}} \boldsymbol{n}_{i,i+1} \otimes \int_{\boldsymbol{r}_i}^{\boldsymbol{r}_{i+1}} \delta\boldsymbol{r}\, \mathrm{d}\ell.\end{aligned} \quad (28)$$

Here the cell outline ∂A is parametrized in terms of the curvilinear coordinate ℓ, $\boldsymbol{n}$ is the local normal unit vector pointing outward from the cell interior, and $\delta\boldsymbol{r}$ is the local virtual displacement of the cell outline. In the second step in Eq. (28), we used that cell outlines are polygons with linear interfaces between vertices.

To carry out the integral over a cell polygon side $i \to i+1$ in Eq. (28), we make the choice to linearly interpolate the virtual displacement $\delta\boldsymbol{r}$ along each polygon side. In other words, at any point $\boldsymbol{r}(\lambda) = (1-\lambda)\boldsymbol{r}_i + \lambda\boldsymbol{r}_{i+1}$, we choose the virtual displacement to be

$$\delta\boldsymbol{r} = (1-\lambda)\delta\boldsymbol{r}_i + \lambda\delta\boldsymbol{r}_{i+1}, \quad (29)$$

where $0 \le \lambda \le 1$. Note that other choices for $\delta\boldsymbol{r}(\lambda)$ are possible as long as $\delta\boldsymbol{r}(0) = \delta\boldsymbol{r}_i$, $\delta\boldsymbol{r}(1) = \delta\boldsymbol{r}_{i+1}$, and the polygon side remains straight. In particular, any tangential (i.e. parallel to the polygon side) component could in principle be added to $\delta\boldsymbol{r}(\lambda)$.

Insertion of Eq. (29) into the integral in Eq. (28) yields:

$$\int_{\boldsymbol{r}_i}^{\boldsymbol{r}_{i+1}} \delta\boldsymbol{r}\, \mathrm{d}\ell = \frac{1}{2} l_{i,i+1}(\delta\boldsymbol{r}_i + \delta\boldsymbol{r}_{i+1}). \quad (30)$$

Using $l_{i,i+1}\boldsymbol{n}_{i,i+1} = (\boldsymbol{r}_{i+1} - \boldsymbol{r}_i) \times \hat{\boldsymbol{z}}$, Eq. (28) can thus be expressed as

$$\int_A \delta\boldsymbol{\varepsilon}\, \mathrm{d}A = \frac{1}{2} \sum_{i\in\mathrm{cell}} \left[(\boldsymbol{r}_{i+1} - \boldsymbol{r}_{i-1}) \times \hat{\boldsymbol{z}}\right] \otimes \delta\boldsymbol{r}_i. \quad (31)$$

Combining this identity with Eqs. (26) and (27), and comparing the coefficients in front of the virtual displacements $\delta\boldsymbol{r}_i$, we finally obtain:

$$\boldsymbol{F}_i^{(X)} = -\frac{1}{2}\left[(\boldsymbol{r}_{i+1} - \boldsymbol{r}_{i-1}) \times \hat{\boldsymbol{z}}\right] \cdot \boldsymbol{\sigma}^{(\mathrm{b})}. \quad (32)$$

This result corresponds to the Tlili scheme: $\boldsymbol{F}_i^{(X)} \equiv \boldsymbol{F}_i^{(T)}$, see Eq. (4). Hence, the Tlili et al. scheme can be obtained like the Comelles et al. scheme yet without the uniform-virtual-strain projection of Eq. (7).

In Eq. (29), we made a choice for the virtual displacements on the polygon sides. Other choices are possible as well and will generally lead to a different force formula. Also note that for given virtual vertex displacements $\delta\boldsymbol{r}_i$, Eq. (29) can always be fulfilled for all polygon sides simultaneously. Meanwhile, the condition of a uniform virtual strain on the cell area may generally not be fulfilled for general displacements δr_i.

6 Neither of the two schemes recapitulates the standard vertex model forces

We wondered whether it would be possible to express the standard vertex model forces $\boldsymbol{F}_i^{(\mathrm{svm})}$ (cf. Eq. (22)) exclusively in terms of a cellular bulk stress $\boldsymbol{\sigma}^{(\mathrm{b})}$.

More generally one could ask whether any set of vertex forces $\boldsymbol{F}_i$ created by a cell can be expressed in terms of a cellular bulk stress $\boldsymbol{\sigma}^{(\mathrm{b})}$. However, because any arbitrary set of vertex forces with vanishing net force and net torque correspond to $(2\times N-2)$ degrees of freedom while $\boldsymbol{\sigma}^{(\mathrm{b})}$ contains only 3 degrees of freedom, this is in general not possible.

We thus focus on the specific question whether one of the two schemes could produce the standard vertex model forces $\boldsymbol{F}_i^{(\mathrm{svm})}$ for some bulk stress $\boldsymbol{\sigma}^{(\mathrm{b})}$. In other words, we ask whether there is a $\boldsymbol{\sigma}^{(\mathrm{b})}$ such that for a scheme $x \in \{T, C\}$:

$$\boldsymbol{F}_i^{(x)}(\boldsymbol{\sigma}^{(\mathrm{b})}) = \boldsymbol{F}_i^{(\mathrm{svm})}. \quad (33)$$

Since both schemes reproduce the correct Batchelor stress (Sec. 2.3), if there was a stress $\boldsymbol{\sigma}^{(\mathrm{b})}$ that could produce the standard vertex model forces $\boldsymbol{F}_i^{(\mathrm{svm})}$, it needs to be the Batchelor stress of $\boldsymbol{F}_i^{(\mathrm{svm})}$. Formally, this can be shown by inserting Eq. (33) into Eq. (16):

$$\boldsymbol{\sigma}^{(\mathrm{b})} = \boldsymbol{\sigma}_B\left[\boldsymbol{F}_i^{(x)}(\boldsymbol{\sigma}^{(\mathrm{b})})\right] = \boldsymbol{\sigma}_B\left[\boldsymbol{F}_i^{(\mathrm{svm})}\right]. \quad (34)$$

To compute this stress, we first explicitly compute the forces $\boldsymbol{F}_i^{(\mathrm{svm})}$:

$$\begin{aligned}\boldsymbol{F}_i^{(\mathrm{svm})} =& -\frac{1}{2} K_A\,(A - A_0)\left[(\boldsymbol{r}_{i+1} - \boldsymbol{r}_{i-1}) \times \hat{\boldsymbol{z}}\right] \\ &+ K_P\,(P - P_0)\,(\boldsymbol{t}_{i,i+1} - \boldsymbol{t}_{i-1,i}),\end{aligned} \quad (35)$$

where $\boldsymbol{t}_{i,i+1} = (\boldsymbol{r}_{i+1} - \boldsymbol{r}_i)/l_{i,i+1}$ is the unit vector pointing from vertex i to vertex $i+1$.

Substituting Eq. (35) into the Batchelor stress expression Eq. (15) leads to

$$\boldsymbol{\sigma}_B\left[\boldsymbol{F}_i^{(\mathrm{svm})}\right] = K_A\,(A - A_0)\,\boldsymbol{I} + \frac{K_P P\,(P - P_0)}{A}\boldsymbol{S}, \quad (36)$$

where $\boldsymbol{S}$ is a symmetric cell shape tensor defined as:

$$\boldsymbol{S} = \frac{1}{P} \sum_{i \in cell} l_{i,i+1} \boldsymbol{t}_{i,i+1} \otimes \boldsymbol{t}_{i,i+1}. \tag{37}$$

For isotropic cells, $\boldsymbol{S} = \boldsymbol{I}/2$.

Finally, we can use the stress expression in Eq. (36) to test whether one of the schemes is able to produce the standard vertex model forces.

Tlili et al. scheme. To compute the vertex forces resulting from the stress in Eq. (36), we insert it into the Tlili scheme, Eq. (4):

$$\begin{aligned} \boldsymbol{F}_i^{(\mathrm{T})} = &- \frac{1}{2} K_A \left(A - A_0\right) \left[\left(\boldsymbol{r}_{i+1} - \boldsymbol{r}_{i-1}\right) \times \hat{\boldsymbol{z}}\right] \\ &- \frac{K_P P \left(P - P_0\right)}{2A} \left[\left(\boldsymbol{r}_{i+1} - \boldsymbol{r}_{i-1}\right) \times \hat{\boldsymbol{z}}\right] \cdot \boldsymbol{S}. \end{aligned} \tag{38}$$

While the area-related term is the same as in Eq. (35), the perimeter-related terms are in general different. Indeed, while for a given vertex i the perimeter part without the factor $(P - P_0)$ in Eq. (35) depends only on the vertex positions $\boldsymbol{r}_{i-1}, \boldsymbol{r}_i, \boldsymbol{r}_{i+1}$, the same part in Eq. (38) depends via $\boldsymbol{S}$ on all vertex positions of the cell. Thus, the Tlili scheme only reproduces the area-related part of the standard vertex model forces.

Comelles et al. scheme. We analogously compute the vertex forces resulting from the stress in Eq. (36) via the Comelles scheme, Eq. (13):

$$\begin{aligned} \boldsymbol{F}_i^{(\mathrm{C})} = &- K_A \left(A - A_0\right) A \boldsymbol{\rho}_i \cdot \boldsymbol{M}^{-1} \\ &- K_P P \left(P - P_0\right) \boldsymbol{\rho}_i \cdot \boldsymbol{M}^{-1} \cdot \boldsymbol{S}. \end{aligned} \tag{39}$$

The latter expression differs from the standard vertex model forces Eq. (35) with respect to both area- and perimeter-related terms. Without the prefactors $(A - A_0)$ and $(P - P_0)$, both terms depend only on the vertex positions $\boldsymbol{r}_{i-1}, \boldsymbol{r}_i, \boldsymbol{r}_{i+1}$ in Eq. (35). However in Eq. (39) both terms generally depend on all vertex positions of the cell.

Taken together, neither of the two schemes allows to represent standard vertex model forces in terms of cellular bulk stresses alone (shown numerically in Appendix C.2). However, the Tlili scheme allows to at least correctly represent the (isotropic) area-related part. In the specific case of a regular polygonal cell, the forces according to both schemes coincide with the standard vertex model forces: $\boldsymbol{F}_i^{(T)} = \boldsymbol{F}_i^{(C)} = \boldsymbol{F}_i^{(\mathrm{svm})}$ (Appendix C.1).

7 Discussion

The vertex model describes tissue mechanics based on vertex motion and vertex forces, raising the question of how cellular bulk stresses can be described in this model. Here we compare two different schemes to transform bulk isotropic and anisotropic stresses into vertex forces: the Tlili et al. scheme proposed in [3] and the Comelles et al. scheme proposed in [4].

We first show analytically that both schemes transform similarly with respect to affine transformations of the cell shape. We then show numerically that nevertheless both schemes lead to different predictions of the vertex model dynamics (Section 4). These differences thus arise from different behaviors of both schemes with respect to non-affine deformations of the cell shape. Moreover, we show analytically that the Tlili et al. scheme can be derived similarly to the Comelles et al. scheme – yet without the affine-virtual-deformation projection that appears in the derivation of the Comelles et al. scheme. Finally, we show that neither scheme allows to fully express standard vertex model forces [17] in terms of bulk cellular stresses alone.

Taken together, our results suggest that both Tlili et al. and Comelles et al. schemes are reasonable choices, as they transform in the same way with respect to affine deformations. As evidenced by the absence (Tlili scheme) or appearance (Comelles scheme) of net forces on vertices for periodic boundary conditions in Section 4, the Tlili scheme describes uniform bulk stresses within each cell, while the Comelles scheme can be interpreted as describing non-uniform stress on the cell area. Nevertheless, as the vertex model is an effective cell-scale description of complex cellular mechanics, both schemes are of interest to model anisotropic cellular bulk stresses in biological tissues.

8 Perspectives

In recent vertex model work, collective cellular migration was most often studied by including a polar variable for each cell that controls cellular self-propulsion [20,21,18,22]. The approaches discussed here allow for another way to include cellular motion into the vertex model, for instance through cellular nematic variables controlling bulk anisotropic stresses. In our numerical studies we have focused on the case of homogeneous bulk stress. However, one may consider spatial variations in the bulk stress amplitude or orientation, which result in forces that can drive tissue flows. Such an implementation of cellular motility is also consistent with recent hydrodynamic descriptions of cell monolayer dy-

namics [23,24,25], in which active anisotropic stresses are controlled by a nematic cell shape field.

Motility can also arise from heterogeneous stresses within cells. For instance, intra-cellular contractility fluctuations have been shown to be correlated to the migratory behavior[26]. It will be interesting to extend our framework to account for such non-uniform bulk stresses at the sub-cellular level. This would allow to explore what types of tissue-scale flow arise from the generic models of cell migration proposed in [26].

Supplementary Movies

Supplementary Movies 1-3 are available as ancillary files.

Acknowledgements

We thank M.M. Inamdar, F. Jülicher, G. Salbreux, D. Riveline, and S. Tlili for useful comments. This project was funded by grants from the Investissements d'Avenir French Government program managed by the French National Research Agency (ANR-16-CONV- 0001 and ANR-20-CE30-0023 COVFEFE) and from Excellence Initiative of Aix-Marseille University - A*MIDEX.

Author Contribution Statement

All authors contributed to deriving the analytical results, writing the paper and conceptualizing the research; S.-Z. L. also carried out the simulations.

References

1. Benoit Ladoux and René Marc Mège. Mechanobiology of collective cell behaviours. *Nature Reviews Molecular Cell Biology*, 18(12):743–757, 2017.
2. Sham Tlili, Cyprien Gay, François Graner, Philippe Marcq, François Molino, and Pierre Saramito. Colloquium: Mechanical formalisms for tissue dynamics, 2015.
3. S. Tlili, J. Yin, J.-F. Rupprecht, M. A. Mendieta-Serrano, G. Weissbart, N. Verma, X. Teng, Y. Toyama, J. Prost, and T. E. Saunders. Shaping the zebrafish myotome by intertissue friction and active stress. *Proceedings of the National Academy of Sciences of the United States of America*, 116(51):25430–25439, 2019.
4. Jordi Comelles, Soumya SS, Linjie Lu, Emilie Le Maout, Sudakar Anvitha, Guillaume Salbreux, Frank Jülicher, Mandar M Inamdar, and Daniel Riveline. Epithelial colonies in vitro elongate through collective effects. *eLife*, 10, jan 2021.
5. Tatsuzo Nagai and Hisao Honda. A dynamic cell model for the formation of epithelial tissues. *Philosophical Magazine Part B*, 81(7):699–719, 2001.
6. Reza Farhadifar, Jens Christian Röper, Benoit Aigouy, Suzanne Eaton, and Frank Jülicher. The Influence of Cell Mechanics, Cell-Cell Interactions, and Proliferation on Epithelial Packing. *Current Biology*, 17(24):2095–2104, 2007.
7. D B Staple, R Farhadifar, J. C. Röper, B. Aigouy, S. Eaton, and F. Jülicher. Mechanics and remodelling of cell packings in epithelia. *The European Physical Journal E*, 33(2):117–127, oct 2010.
8. Alexander G Fletcher, James M Osborne, Philip K Maini, and David J Gavaghan. Implementing vertex dynamics models of cell populations in biology within a consistent computational framework. *Progress in Biophysics and Molecular Biology*, 113(2):299–326, 2013.
9. Dapeng Bi, J. H. Lopez, J. M. Schwarz, and M. Lisa Manning. A density-independent rigidity transition in biological tissues. *Nature Physics*, 11(12):1074–1079, 2015.
10. Silvanus Alt, Poulami Ganguly, and Guillaume Salbreux. Vertex models: From cell mechanics to tissue morphogenesis. *Philosophical Transactions of the Royal Society B: Biological Sciences*, 372(1720), 2017.
11. Matteo Rauzi, Pierre-françois Lenne, and Thomas Lecuit. Planar polarized actomyosin contractile flows control epithelial junction remodelling. *Nature*, 468(7327):1110–1114, 2010.
12. Benoit Dehapiot, Raphaël Clément, Hervé Alégot, Gabriella Gazsó-Gerhát, Jean Marc Philippe, and Thomas Lecuit. Assembly of a persistent apical actin network by the formin Frl/Fmnl tunes epithelial cell deformability. *Nature Cell Biology*, 22(7):791–802, 2020.
13. R. Penrose. A generalized inverse for matrices. *Mathematical Proceedings of the Cambridge Philosophical Society*, 51(3):406–413, 1955.
14. G. K. Batchelor. The stress system in a suspension of force-free particles. *Journal of Fluid Mechanics*, 41(3):545–570, 1970.
15. A. W. C. Lau and T. C. Lubensky. Fluctuating hydrodynamics and microrheology of a dilute suspension of swimming bacteria. *Physical Review E*, 80(1):011917, 2009.
16. Alexander Nestor-Bergmann, Georgina Goddard, Sarah Woolner, and Oliver E Jensen. Relating cell shape and mechanical stress in a spatially disordered epithelium using a vertex-based model. *Mathematical Medicine and Biology*, 35:1–27, 2018.
17. Reza Farhadifar, Jens-Christian Röper, Benoit Aigouy, Suzanne Eaton, and Frank Jülicher. The influence of cell mechanics, cell-cell interactions, and proliferation on epithelial packing. *Current Biology*, 17(24):2095–2104, 2007.
18. Shao Zhen Lin, Sang Ye, Guang Kui Xu, Bo Li, and Xi Qiao Feng. Dynamic migration modes of collective cells. *Biophysical Journal*, 115(9):1826–1835, 2018.
19. Matthias Merkel, Raphaël Etournay, Marko Popović, Guillaume Salbreux, Suzanne Eaton, and Frank Jülicher. Triangles bridge the scales: Quantifying cellular contributions to tissue deformation. *Physical Review E*, 95(3):032401, mar 2017.
20. Dapeng Bi, Xingbo Yang, M Cristina Marchetti, and M Lisa Manning. Motility-Driven Glass and Jamming Transitions in Biological Tissues. *Physical Review X*, 6(2):021011, apr 2016.
21. Fabio Giavazzi, Matteo Paoluzzi, Marta Macchi, Dapeng Bi, Giorgio Scita, Lisa Manning, Roberto Cerbino, and M. Cristina Marchetti. Flocking Transitions in Confluent Tissues. *Soft Matter*, 2018.
22. Matteo Paoluzzi, Luca Angelani, Giorgio Gosti, M Cristina Marchetti, Ignacio Pagonabarraga, and Giancarlo Ruocco. Alignment interactions drive structural

transitions in biological tissues. *arXiv:2107.00523*, pages 1–15, jul 2021.
23. Thuan Beng Saw, Amin Doostmohammadi, Vincent Nier, Leyla Kocgozlu, Sumesh Thampi, Yusuke Toyama, Philippe Marcq, Chwee Teck Lim, Julia M. Yeomans, and Benoit Ladoux. Topological defects in epithelia govern cell death and extrusion. *Nature*, 544(7649):212–216, 2017.
24. Kyogo Kawaguchi, Ryoichiro Kageyama, and Masaki Sano. Topological defects control collective dynamics in neural progenitor cell cultures. *Nature*, 545(7654):327–331, 2017.
25. G Duclos, C. Blanch-Mercader, V Yashunsky, G Salbreux, J. F. Joanny, J Prost, and P. Silberzan. Spontaneous shear flow in confined cellular nematics. *Nature Physics*, 14(7):728–732, jul 2018.
26. Paolo Maiuri, Jean-François Rupprecht, Stefan Wieser, Verena Ruprecht, Olivier Bénichou, Nicolas Carpi, Mathieu Coppey, Simon De Beco, Nir Gov, Carl-Philipp Heisenberg, Carolina Lage Crespo, Franziska Lautenschlaeger, Maël Le Berre, Ana-Maria Lennon-Dumenil, Matthew Raab, Hawa-Racine Thiam, Matthieu Piel, Michael Sixt, and Raphaël Voituriez. Actin Flows Mediate a Universal Coupling between Cell Speed and Cell Persistence. *Cell*, 161(2):374–386, 2015.

Appendix A: Cell and tissue aspect ratio change

In Figs. 2 and 3, we have quantified the relative cell aspect ratio change as $\varepsilon_{\rm cell} = {\rm AR}_{\rm final}/{\rm AR}_{\rm initial} - 1$, where ${\rm AR}_{\rm initial}$ (${\rm AR}_{\rm final}$) is the aspect ratio of the cell in the initial (final) state. AR is defined as ${\rm AR} = \sqrt{I_1/I_2}$, where I_1 and I_2 ($I_1 > I_2$) are the two eigenvalues of the matrix $\boldsymbol{M}$ defined in Eq. (11).

Similarly, for free boundary conditions, we analogously define the relative tissue aspect ratio change $\varepsilon_{\rm tissue}$. In this case however, the tensor $\boldsymbol{M}$ is defined via Eq. (11) using all margin vertices of the tissue.

Appendix B: Consistency checks

Appendix B.1: Zero net force and torque across each cell

Zero net force We check that the net force on all vertices of a cell satisfies the relation

$$\boldsymbol{F}_G = \sum_{i\in cell} \boldsymbol{F}_i^{(T,C)} = \boldsymbol{0}, \tag{B.1}$$

in both schemes. Indeed, substituting the Tlili et al. forces Eq. (4) into Eq. (B.1), we find that

$$\boldsymbol{F}_G = \frac{1}{2}\left[\hat{\boldsymbol{z}} \times \sum_{i\in cell} (\boldsymbol{r}_{i+1} - \boldsymbol{r}_{i-1})\right] \cdot \boldsymbol{\sigma}^{(\rm b)} = \boldsymbol{0}, \tag{B.2}$$

Table 1 List of parameter values used in vertex model simulation.

Parameter	Description	Value
$\sqrt{A_0}$	Length scale	1.0
$\gamma/(K_A A_0)$	Time scale	1.0
$K_A A_0$	Stress scale	1.0
K_A	Cell area elasticity	1.0
A_0	Cell target area	1.0
K_P	Cell perimeter elasticity	0.02
P_0	Preferred perimeter	-2.5
$\Delta_{\rm T1}$	Length threshold for T1 transition	0.01
Δt	Simulation time step	0.01

Likewise, substitution of the Comelles et al. definitions Eq. (13) into Eq. (B.1) leads to

$$\sum_{i\in cell} \boldsymbol{F}_i^{(C)} = -A\left(\sum_{i\in cell} \boldsymbol{\rho}_i\right) \cdot \boldsymbol{M}^{-1} \cdot \boldsymbol{\sigma}^{(\rm b)} = \boldsymbol{0}. \tag{B.3}$$

Zero net torque We also check that the overall torque acting on a given cell satisfies the relation

$$\boldsymbol{T} = \sum_{i\in cell} \boldsymbol{r}_i \times \boldsymbol{F}_i^{(T,C)} = 0 \tag{B.4}$$

in both schemes. Substituting the Tlili et al. scheme definition Eq. (4) into Eq. (B.4), and adopting Einstein notation with Greek dimension indices, we obtain:

$$T_\alpha = -\frac{1}{2}\sum_{i\in cell} \varepsilon_{\alpha\beta\gamma} r_{i,\beta} \varepsilon_{\eta z\mu} (r_{i+1,\eta} - r_{i-1,\eta}) \sigma^{(b)}_{\mu\gamma}. \tag{B.5}$$

To further simplify this expression, we note that:

$$\sum_{i\in cell} r_{i,\beta} \varepsilon_{\eta z\mu} (r_{i+1,\eta} - r_{i-1,\eta}) = 2A\delta_{\beta\mu}. \tag{B.6}$$

This relation can be verified by testing each dimension index combination for the pair (β, μ). Using Eq. (B.6) in Eq. (B.5), we find that

$$T_\alpha = -A\varepsilon_{\alpha\beta\gamma}\sigma^{(b)}_{\beta\gamma}. \tag{B.7}$$

For symmetric bulk stress tensors $\boldsymbol{\sigma}^{(\rm b)}$, we thus obtain $\boldsymbol{T} = \boldsymbol{0}$.

Substitution of the Comelles et al. force definition Eq. (13) into Eq. (B.4), adopting index notation, yields

$$\begin{aligned} T_\alpha &= -A\varepsilon_{\alpha\beta\gamma}M^{-1}_{\eta\mu}\sigma^{(b)}_{\mu\gamma}\sum_{i\in cell} r_{i,\beta}\rho_{i,\eta}, \\ &= -A\varepsilon_{\alpha\beta\gamma}M^{-1}_{\eta\mu}\sigma^{(b)}_{\mu\gamma}\sum_{i\in cell} \rho_{i,\beta}\rho_{i,\eta}, \\ &= -A\varepsilon_{\alpha\beta\gamma}M_{\beta\eta}M^{-1}_{\eta\mu}\sigma^{(b)}_{\mu\gamma}, \\ &= -A\varepsilon_{\alpha\beta\gamma}\sigma^{(b)}_{\beta\gamma}. \end{aligned} \tag{B.8}$$

Hence, again, for symmetric $\boldsymbol{\sigma}^{(\mathrm{b})}$, the overall torque is zero: $\boldsymbol{T} = \boldsymbol{0}$.

Appendix B.2: Self-consistency: the input bulk stress equals the output Batchelor stress

Here we show that in both schemes, the Batchelor stress Eq. (15) is identical to the input bulk cell-stress $\boldsymbol{\sigma}^{(\mathrm{b})}$, i.e. that: $\boldsymbol{\sigma}_B\left[\boldsymbol{F}_i^{(T,C)}\right] = \boldsymbol{\sigma}^{(\mathrm{b})}$.

Substituting the Tlili et al. force expression Eq. (4) into Eq. (15) we immediately obtain:

$$\begin{aligned} \boldsymbol{\sigma}_B\left[\boldsymbol{F}_i^{(T)}\right] &= \frac{1}{2A}\sum_{i\in cell} \boldsymbol{r}_i \otimes \left[(\boldsymbol{r}_{i+1}-\boldsymbol{r}_{i-1})\times\hat{\boldsymbol{z}}\right]\cdot\boldsymbol{\sigma}^{(\mathrm{b})} \\ &= \boldsymbol{\sigma}^{(\mathrm{b})}, \end{aligned} \tag{B.9}$$

where in the second step, we have applied Eq. (B.6).

Similarly, substitution of the Comelles et al. force definition Eq. (13) into Eq. (15) leads to

$$\begin{aligned} \boldsymbol{\sigma}_B\left[\boldsymbol{F}_i^{(C)}\right] &= -\frac{1}{A}\sum_{i\in cell} \boldsymbol{r}_i \otimes \left[-A\boldsymbol{\rho}_i\cdot\boldsymbol{M}^{-1}\cdot\boldsymbol{\sigma}^{(\mathrm{b})}\right] \\ &= \left(\sum_{i\in cell}\boldsymbol{r}_i\otimes\boldsymbol{\rho}_i\right)\cdot\boldsymbol{M}^{-1}\cdot\boldsymbol{\sigma}^{(\mathrm{b})}, \\ &= \left(\sum_{i\in cell}\boldsymbol{\rho}_i\otimes\boldsymbol{\rho}_i\right)\cdot\boldsymbol{M}^{-1}\cdot\boldsymbol{\sigma}^{(\mathrm{b})} \\ &= \boldsymbol{\sigma}^{(\mathrm{b})}. \end{aligned} \tag{B.10}$$

with the matrix $\boldsymbol{M}$ defined in Eq. (11).

Appendix C: Capacity of both schemes to reproduce standard vertex model forces

Appendix C.1: Identity of forces for regular polygonal cells

Here we consider a regular polygonal cell composed of N vertices $\{\boldsymbol{r}_i\}_{i=1,\dots,N}$ with $\boldsymbol{r}_i = r\boldsymbol{e}_i$, with $r>0$, $\boldsymbol{e}_i = (\cos\theta_i, \sin\theta_i)$, and the vertex angles $\theta_i = 2(i-1)\pi/N$. Area and perimeter of such a cell are:

$$A = \frac{1}{2}Nr^2\sin\left(\frac{2\pi}{N}\right), \tag{C.11}$$

$$P = 2Nr\sin\left(\frac{\pi}{N}\right). \tag{C.12}$$

To simplify the standard vertex model forces Eq. (35), we use the relations

$$(\boldsymbol{r}_{i+1}-\boldsymbol{r}_{i-1})\times\hat{\boldsymbol{z}} = 2r\sin\left(\frac{2\pi}{N}\right)\boldsymbol{e}_i \tag{C.13}$$

$$\boldsymbol{t}_{i,i+1}-\boldsymbol{t}_{i-1,i} = -2\sin\left(\frac{\pi}{N}\right)\boldsymbol{e}_i \tag{C.14}$$

and obtain:

$$\begin{aligned} \boldsymbol{F}_i^{(\mathrm{svm})} =& -K_A(A-A_0)r\sin\left(\frac{2\pi}{N}\right)\boldsymbol{e}_i \\ & -2K_P(P-P_0)\sin\left(\frac{\pi}{N}\right)\boldsymbol{e}_i. \end{aligned} \tag{C.15}$$

The Tlili et al. vertex forces in Eq. (38) simplify since we consider regular hexagons and thus $\boldsymbol{S} = \boldsymbol{I}/2$. Inserting Eqs. (C.11), (C.12) and (C.13) in Eq. (36), we recover indeed an expression identical to the one in Eq. (C.15).

To compute the Comelles et al. forces, we fist evaluate each component of the $\boldsymbol{M}$ tensor defined in Eq. (11). We find for $N \geq 3$:

$$\begin{aligned} M_{xx} &= r^2\sum_{i=1}^{N}\cos^2\theta_i = \frac{1}{2}r^2\sum_{i=1}^{N}(1+\cos 2\theta_i) = \frac{N}{2}r^2, \\ M_{yy} &= r^2\sum_{i=1}^{N}\sin^2\theta_i = \frac{1}{2}r^2\sum_{i=1}^{N}(1-\cos 2\theta_i) = \frac{N}{2}r^2, \end{aligned}$$

while

$$M_{xy} = r^2\sum_{i=1}^{N}\cos\theta_i\sin\theta_i = \frac{1}{2}r^2\sum_{i=1}^{N}\sin 2\theta_i = 0,$$

which leads to $\boldsymbol{M} = Nr^2/2\ \boldsymbol{I}$. Therefore, the vertex forces given by the Comelles et al. scheme are

$$\boldsymbol{F}_i^{(\mathrm{C})} = -r\sin\left(\frac{2\pi}{N}\right)\boldsymbol{e}_i\cdot\boldsymbol{\sigma}_B\left[\boldsymbol{F}_i^{(\mathrm{svm})}\right]. \tag{C.16}$$

Injecting the stress expression Eq. (36) into Eq. (C.16), we find that the Comelles et al. expression is identical to Eq. (C.15); thus $\boldsymbol{F}_i^{(\mathrm{T})} = \boldsymbol{F}_i^{(\mathrm{C})} = \boldsymbol{F}_i^{(\mathrm{svm})}$ for regular polygonal cells.

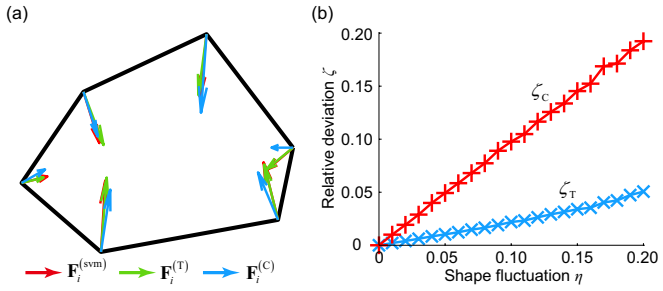

Fig. 4 Differences between the forces according to both schemes and the standard vertex model forces for irregular cell shapes. Vertex positions correspond to a randomly perturbed hexagonal cell according to Eq. (C.17). (a) The Tlili et al. forces $\boldsymbol{F}_i^{(\mathrm{T})}$ (green arrows), the Comelles et al. forces $\boldsymbol{F}_i^{(\mathrm{C})}$ (blue arrows), and the standard vertex model forces $\boldsymbol{F}_i^{(\mathrm{svm})}$ (red arrows) at each cell vertex for an example configuration. (b) Dependence of the relative force deviations ζ_{T} and ζ_{C} defined in Eq. (C.18) on the amplitude η of the deviation of the cell shape from a regular hexagonal shape. Vertex model parameters are provided in Table 1.

Appendix C.2: Numerical comparison of forces for irregular hexagons

We numerically compare the Tlili et al. and Comelles et al. forces with the standard vertex model forces for non-regular hexagonal cells. We define the corners of the hexagonal cell as $\boldsymbol{r}_i = (x_i, y_i)$ with $i = 1, 2, \cdots, 6$ and:

$$x_i = \cos\frac{i\pi}{3} + \eta\vartheta_{ix}, \qquad y_i = \sin\frac{i\pi}{3} + \eta\vartheta_{iy}. \tag{C.17}$$

Here, ϑ_{ix} and ϑ_{iy} are independent, zero-mean, unit-variance Gaussian random variables, and η is a parameter tuning the deviation of the cell shape from that of a regular hexagon.

Discrepancies between the two schemes and the standard vertex model forces are quantified in terms of

$$\zeta_X = \left\langle \left| \boldsymbol{F}_i^{(X)} - \boldsymbol{F}_i^{(\mathrm{svm})} \right| / \left| \boldsymbol{F}_i^{(\mathrm{svm})} \right| \right\rangle, \tag{C.18}$$

where $X \in \{T, C\}$, indicating Tlili and Comelles et al. schemes, respectively. The average $\langle\cdot\rangle$ is over all cell vertices and over $1,000$ realizations for the set of the Gaussian random variables ϑ_{ix} and ϑ_{iy}.

We find that the deviations of both Tlili et al. and Comelles et al. forces from the standard vertex model forces increase with increasing cell shape deviation from a regular hexagonal shape, see Fig. 4b. However, the Tlili et al. forces deviated less from the standard vertex model forces than the Comelles et al. forces did.